RSC Advances

PAPER

View Article Online
View Journal | View Issue

Cite this: *RSC Adv.*, 2024, **14**, 31694

Sustained antibacterial release of zwitterionic globular hyperbranched polymer dots intercalated into layered double hydroxides†

Chun-Kuei Liu,[a] Fang-Yi Su,[a] Tzong-Yuan Juang *[b] and Yung-Chuan Liu*[a]

Received 1st August 2024
Accepted 27th September 2024

DOI: 10.1039/d4ra05587j

rsc.li/rsc-advances

This study introduces zwitterionic hyperbranched polymer (HBP) dots intercalated into layered double hydroxides (LDHs) for sustained antibacterial release. The proposed zwitterionic HBPs possess a three-dimensional spherical structure; unconventional blue fluorescent luminescence; water solubility; abundant COOH, amine, and amide functional groups; anionic exchangeability for intercalating into LDH interlayers; and sustained-release antibacterial activity. The intercalation for the layered nanomaterials was determined by adding different weight ratios of HBPs to Mg–Al LDHs to investigate the changes in the interlayer distance. X-ray diffraction revealed that the LDH layer spacing increased from 8.6 to 25.5 Å, effectively expanding the interlayer spacing with increasing HBP intercalation. Additionally, Fourier-transform infrared spectroscopy revealed the functional groups of the intercalated nanohybrids. Because the peripheral functional groups of HBPs are amino ($-NH_2$) groups, preliminary evaluations revealed that pristine HBPs exhibited antibacterial properties. We further examined the antibacterial properties of the HBP/LDH nanohybrids. The results showed that HBPs combined with LDHs' controllable release properties can effectively achieve long-term sustained antibacterial release.

1 Introduction

The combination of organic polymers with inorganic layered clays as multifunctional nanostructured materials has recently become a hot research topic.[1–3] One approach involves intercalating organic molecules into layered nanomaterials, which enables their broad range of applications in catalysis, adsorption, and biomedical science.[4–7]

Hyperbranched polymers (HBPs) are compounds that lie between crosslinked and branched polymers[8,9] and possess highly branched three-dimensional organic structures, abundant end functional groups, and good solubility in solutions. Their highly branched three-dimensional spherical nanostructures render HBPs as being ideal candidates for various applications. Notably, because of their spherical and internally hollow structures, HBPs can be utilized for drug encapsulation and can serve as excellent nanocontainers that can accommodate a diverse range of molecules.[10] Additionally, different noncovalent interactions, such as hydrophobic interactions, hydrogen bonding, and ionic interactions,[8,11,12] can be utilized to change the external functional groups and, thus, alter the physicochemical properties of HBPs. Furthermore, drugs in HBP-based drug systems can be delivered by conjugation with drugs in HBPs. For example, in active targeting, a target site directly attached to the nanocarrier surface is inserted into the drug delivery system for increasing the cellular uptake of the nanocarrier to effectively deliver its drugs and enhance the cellular specificity.[13] These cell-targeting modalities specifically interact with receptors on endothelial cells from which cancer or blood vessels arise, enhancing nanocarrier binding and rendering active cell targeting particularly useful for cancer treatment because of the reduced delivery of potentially toxic drugs to healthy tissues.[8,14]

Anionic clays, layered double hydroxides (LDHs), also known as hydrotalcite-like materials, are natural minerals and easily synthesized in the laboratory. LDHs exhibit high adsorption capacities and affinities for various anions, including OH^-, Cl^-, and NO_3^-, and organic anions, such as benzoate or adipate, and even complex biomolecules, such as drug molecules and DNA.[15,16] These anions interact with the interlayer space of LDHs. A series of nanomaterials assembled through intercalation with various compounds is referred to as layered nanohybrids.[4,7,17–19]

Because of their layered structures and exchangeable interlayer ions, LDHs are a class of compounds possessing charge interactions between layers, allowing for ion exchange.[16,17,20] This property enables LDHs to possess positively charged surfaces balanced by interlayer hydrated anions. Ion exchange is crucial

[a]*Department of Chemical Engineering, National Chung Hsing University, 145 Xingda Rd., South Dist., Taichung, 40227, Taiwan. E-mail: ycliu@dragon.nchu.edu.tw; Fax: +886-4-22854734; Tel: +886-4-22853769*

[b]*Department of Cosmeceutics, China Medical University, Taichung, 40402, Taiwan. E-mail: tyjuang@mail.cmu.edu.tw; Tel: +886-4-22053366-5312*

† Electronic supplementary information (ESI) available. See DOI: https://doi.org/10.1039/d4ra05587j

for synthesizing LDHs with larger anionic clusters. Through the control of parameters such as temperature and pH during ion exchange, not only the original lattice structure of LDHs can be preserved but also the types and quantities of interlayer anions can be designed and assembled. In the presence of strong polar molecules, the ion exchange or intercalation of layered compounds can be utilized to synthesize many complexes. For instance, the intercalation of folic acid, used to treat various forms of cancer and prevent vitamin deficiencies, may be possible.[17] In controllable release systems, the resulting nanohybrids could reduce the continuous release of drug doses during the disease treatment, thereby prolonging their effectiveness. Furthermore, LDHs are also applied in water treatment for adsorbing and removing pollutants, such as heavy metal ions and organic pollutants, which are important for improving water quality and environmental protection.[21,22] LDHs are also employed in nanocatalysis to enhance the efficiency and selectivity of chemical reactions, promoting green and sustainable chemical syntheses.[23] LDHs play important roles in environmental applications, agricultural improvement, and biomedical applications, all of which address contemporary challenges and demonstrate more advanced applications.[6,17,24,25]

In this study, we intercalated zwitterionic globular HBPs into LDH interlayers by embedding HBPs within Mg–Al LDH nanolayers *via* ion exchange. The resulting nanostructured hybrids exhibited ion exchange and pH-responsive controlled release properties. We explored their antibacterial efficacies and investigated the temporal aspects of their effectiveness.

2 Materials and methods

2.1 Chemicals and instruments

All the chemicals used in the experiments were analytical grade. Nutrient agar was obtained from Difco™, BD. Lysogeny broth (LB) was purchased from Miller, Scharlau. Ampicillin (Amp50) sodium salt and quinine sulfate dihydrate were purchased from Sigma-Aldrich, and ethylenediaminetetraacetic dianhydride (EDTAD) was purchased from TCI. Jeffamine® T-403 polyetheramine (T403) was purchased from Huntsman, and *N*,*N*-dimethyl formamide (DMF) was purchased from Duksan. Tetrahydrofuran (THF) was purchased from Macron. Magnesium nitrate hexahydrate ($Mg(NO_3)_2 \cdot 6H_2O$) was obtained from Merck. Aluminum nitrate enneahydrate ($Al(NO_3)_3 \cdot 9H_2O$), sodium hydroxide (NaOH), and hydrochloric acid (HCl) were procured from local dealers.

The instruments utilized in this study included a thermal field emission scanning electron microscope (FE-SEM; 7800F, JSM), a superconducting magnet nuclear magnetic resonance spectrometer (NMR; 600/54, Agilent Technologies), a transmission electron microscope (TEM; JEM-1400, JEOL), and a cryogenic scanning electron microscope (SEM; JSM-6700F, JEOL).[26–28]

2.2 Synthesis and characterization of HBPs

We used an $A_2 + B_3$ strategy for the one-pot syntheses of the HBPs.[29] Briefly, T403 and EDTAD were adopted as the A_2 and B_3 molecules, respectively. A THF solution of T403 was added dropwise to the EDTAD solution (at approximately 1 drop per second) under nitrogen at 0 °C. Then, the mixture was continuously stirred and slowly warmed to room temperature. Upon the completion of the reaction, the product was filtered and dried in a vacuum oven at 60 °C for 24 h to yield the HBPs. The critical aspects of the chemical structural features (Fig. 2(a)), NMR and molecular weight of HBPs were thoroughly characterized in our previous study.[30] The molecular weights of the HBPs were determined to be greater than 3500 Da, based on dialysis methods, as their insolubility in THF and DMF *via* GPC measurement.[30]

2.3 Preparation of LDHs

To synthesize the Mg–Al nitrate LDHs, deionized water was boiled to eliminate any CO_2. Magnesium and aluminum nitrates were thoroughly mixed at a 2/1 molar ratio and completely dissolved in the boiling deionized water. The aqueous solution was then cooled to approximately 60 °C and stirred under N_2 to minimize the CO_2 content. Subsequently, the solution pH was adjusted to 10 ± 0.2. The mixture was stirred continuously at 60 °C under N_2 for 16 h. After the completion of the reaction, the solution was centrifuged to remove the water. The resulting white precipitate, Mg–Al nitrate LDHs, was stored in a refrigerator at 4 °C for 12 h.[16,17]

2.4 Preparation of HBP-intercalated LDHs

LDH solutions (64, 32, and 16 mg mL^{-1}) were uniformly mixed with an HBP solution (32 mg mL^{-1}) at HBP/LDH weight ratios of 2/1, 1/1, and 1/2. The mixtures were continuously stirred under N_2 at 80 °C for one day. The resulting precipitates obtained from centrifugation were the HBP/LDH nanocomposite materials.

2.5 Assays

2.5.1 Quantum yield. Quantum yield (QY) refers to the ratio of molecules in the excited state that return to the ground state by emitting fluorescence[31] and is expressed as a fraction of the total number of molecules in the excited state as follows:

$$\Phi_X = \Phi_R\,(I_X/I_R)(A_R/A_X)(\eta_X/\eta_R)^2, \quad (1)$$

where Φ represents the QY; I represents the integrated area of the fluorescence emission spectrum; A is the absorbance at the excitation wavelength in the absorption spectrum; and η is the refractive index of the solution. Subscripts R and X represent the standard and sample, respectively. The standard refers to quinine sulfate dissolved in 0.1 M aqueous H_2SO_4, possessing a QY (Φ_R) of 54%.

2.5.2 Analysis of interlayer spacing. X-rays are emitted because of transitions in the inner electron shells of atoms impacted by high-velocity electrons.[32] When light scatters within a crystal lattice possessing an orderly arrangement of atoms, interference occurs. If the distance between scattering centers is on the same order of magnitude as the wavelength of the incident X-rays, the X-rays diffract.

Bragg's Law is an equation that describes the relationship between the X-ray diffraction angle and spacing between crystal atomic layers. According to Bragg's Law, X-rays constructively interfere when the parameters satisfy the Bragg equation as follows:

$$2d \sin \theta = n\lambda, \quad (2)$$

where d represents the separation spacing between parallel atomic planes in a crystal, and λ and θ are the wavelength and angle of the incident light, respectively.

2.5.3 Antibacterial activity. The antibacterial activity was analyzed using the following approach:[33] *Escherichia coli* (*E. coli*, pUC19/DH5α strain, was gifted from Prof. Cheng at NCHU) was streaked on LB agar containing 50 μg mL^{-1} of Amp50 and incubated at 37 °C for 16 h. A single colony was inoculated in 5 mL of LB containing Amp50 and incubated at 37 °C for 16 h. A 200 μL aliquot of the resulting bacterial culture was inoculated in 5 mL of LB broth containing Amp50 and cultured at 37 °C until OD_{600} reached 0.7 (approximately 2.5 h). Subsequently, 150 μL of the bacterial culture was mixed with 5 mL of 0.75% sterile agar at approximately 45 °C, poured into a culture dish, and allowed to solidify at room temperature before use.

For the antimicrobial activity assay, 10 μL of the test sample solution was dropped onto the agar plate with the bacterial lawn. The plates were then placed in a constant-temperature incubator at 37 °C for 16, 24, 48, and 72 h. Inhibition zones were observed and recorded, and the inhibition zone sizes were measured.

2.5.4 Cell viability. This study chose normal human cells as the research focus. The ability of HBP/LDH to repair skin cells was evaluated using human epidermal keratinocytes (HaCaTs) to assess HBP/LDH wound-healing potential.

HaCaTs were incubated at 5×10^3 cells per well in a 96-well plate for 24 h to allow for cell adhesion. Then, different HBP/LDH concentrations were added to the wells, and the plate was reincubated for an additional 24 h. Subsequently, 3-(4,5-dimethylthiazol-2-yl)-2,5-diphenyltetrazolium bromide (MTT) solution (20 μL per well) was added, and the plate was reincubated for another 3 h. The supernatant was removed, 200 μL of dimethyl sulfoxide (DMSO) solution was added, and the absorbances were measured at 570 nm using a spectrophotometer.[34,35]

3 Results and discussion

3.1 Characteristics of HBP-intercalated LDHs (HBP/LDH)

3.1.1 XRD assay. XRD was utilized to examine the crystal structures of the HBP/LDH prepared at weight ratios of 2/1, 1/1, and 1/2. As shown in Fig. 1, the interlayer spacing was 8.7 Å for the LDHs.[36] According to previous research, the HBP diameter is approximately 2.7 nm.[30] For different weight ratios, signals appeared at approximately 3°–4°, indicating interlayer spacings of 21.8–25.5 Å.[37] With increasing HBP intercalation, the signal corresponding to the intercalated interlayer spacing intensified. In comparison, the XRD pattern of the pristine LDHs exhibited a signal at 10.4°, which disappeared after intercalation,

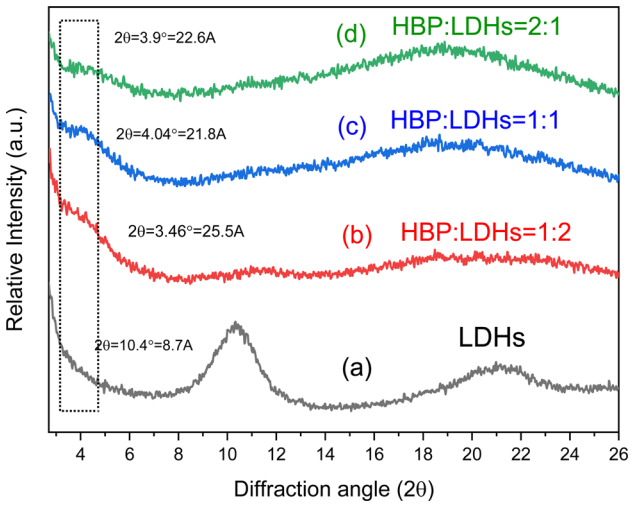

Fig. 1 XRD patterns of (a) pristine LDHs and HBP/LDH = (b) 1/2, (c) 1/1, and (d) 2/1.

indicating that the 3D HBPs clearly intercalated the interlayer space, expanding the interlayer spacing and shifting the peak.[37]

These XRD patterns suggest that HBPs intercalated the LDHs. The LDH interlayer spacing was extended from 8.0 to approximately 24 Å or more. Fig. 2 shows a schematic of the HBP intercalation of LDHs. It is noteworthy that the interlayer spacing of LDH did not increase in proportion to the relative increase in the amount of the intercalating HBP. This phenomenon may be attributed to two factors: the strong interlayer attraction forces inherent to LDH and the globular structural characteristics of the intercalated HBPs. First, the interlayer attraction forces in LDH are inherently stronger than other cation-exchange clays, such as montmorillonite and mica,[16,17,20] which may result in only partial HBP intercalation. Second, the size and branching of HBPs may limit their ability to fully expand the interlayer spacing.[38] The three-dimensional spherical structure of HBP, with a molecular weight exceeding 3500, likely restricts its ability to fully penetrate the confined interlayer spaces of LDH, even when higher concentrations are used to drive the intercalation process. Above effect can limit the extent of LDH interlayer expansion during HBP intercalation.

3.1.2 FTIR assay. The Fourier-transform infrared (FTIR) spectra of the HBP-intercalated LDHs prepared at different weight ratios (w/w) are shown in Fig. 3. The spectrum of the pristine LDHs exhibited O–H and NO_3^- stretching peaks at 3468 and 1384 cm^{-1}, respectively.[39] In the spectra of the HBP/LDH prepared at different weight ratios, these signals weakened at the same positions, and signals appeared at 1664 and 1582 cm^{-1}, corresponding to C=O stretching peaks and amide bonds, suggesting that in the HBP/LDH prepared at different weight ratios, the HBP carboxyl and amide functional groups exchanged anions with NO_3^-, releasing NO_3^- into the solution and weakening the NO_3^- signal. Moreover, signals corresponding to C=O stretching peaks and amide bonds emerged.

3.1.3 Fluorescence assay. The intercalation of different weight ratios of HBPs into LDHs was verified based on the

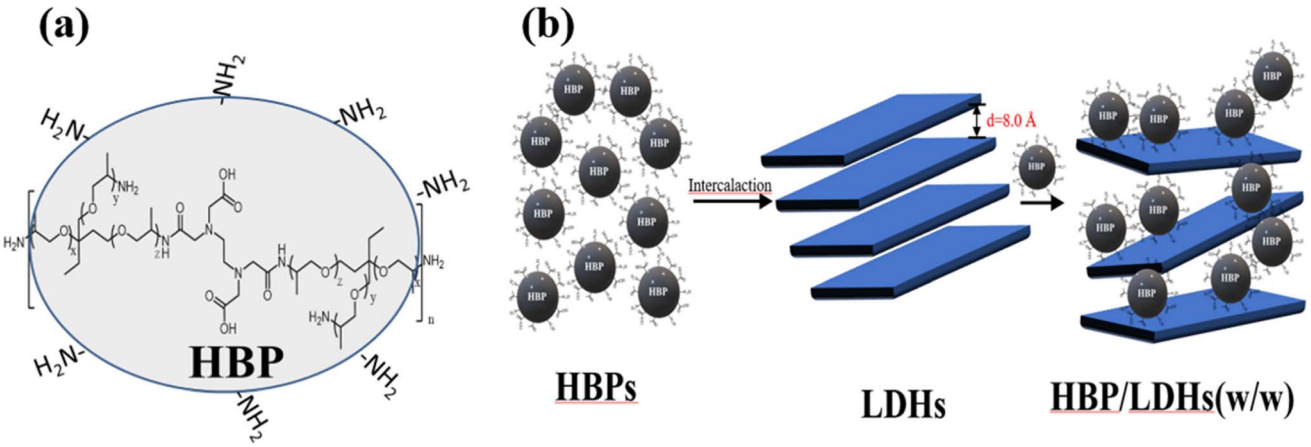

Fig. 2 Schematic of (a) HBP chemical structure and (b) HBP intercalation of LDHs.

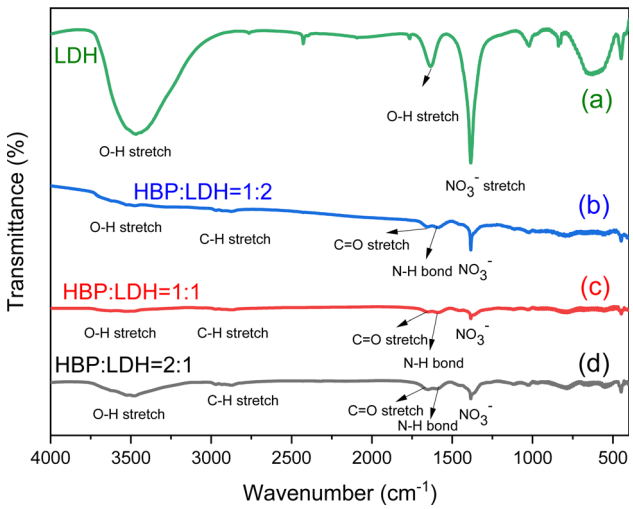

Fig. 3 FTIR spectra of (a) pristine LDHs and HBP/LDH = (b) 1/2, (c) 1/1, and (d) 2/1.

unconventional fluorescence of HBPs (Fig. S1†). Fig. S2† shows the intercalation of different weight ratios of HBPs into LDHs according to the fluorescence observed in daylight and under ultraviolet (UV) light. Clearly, these samples still exhibited fluorescence under UV light irradiation (at 360 nm). Therefore, the Tyndall effect confirmed that the solution contained nanoparticles.

UV-visible (vis) spectra were employed to analyze the intercalation of different weight ratios of HBPs into LDHs. In the range 200–300 nm, C=O π–π^* transitions appeared, while n–π^* transitions appeared in the range 300–400 nm, indicating the presence of carbonyl or amino groups in the LDH solution (Fig. S3†),[30] which contained HBP nanoparticles and exhibited unconventional fluorescence behavior.

In previous studies, HBPs exhibited optimal emission at a wavelength of 360 nm.[30] In this study, HBPs (pH 10) were used to intercalate LDHs at different weight ratios and observe their fluorescence. As shown in Fig. S3,† different weight ratios of HBPs were intercalated into the LDHs, and all the samples showed good linear fluorescence within the margin of error and emission at 440 nm. However, compared with the fluorescence detected at different HBP concentrations in previous studies, the fluorescence of the HBP solution substantially weakened after the HBPs were intercalated into the LDHs, suggesting that the HBPs had intercalated the LDH interlayer and that the corresponding fluorescence weakened because the LDH interlayers blocked the HBP fluorescence.

3.2 Photoluminescence of HBP/LDH at different pH values

As mentioned in Section 3.1.3, the intercalation of HBPs into the LDHs substantially weakens the HBP fluorescence. Next, we adjusted the solution pH after intercalation and observed the resulting HBP fluorescence. As shown in Fig. S2,† after different weight ratios of HBPs were intercalated into LDHs, the solution (pH 10) appeared white and turbid in daylight but exhibited fluorescence under UV light. Upon adjusting the solution pH to 7 and 4, the solution gradually appeared clearer in daylight and maintained fluorescence under UV light. Further observation of the fluorescence during excitation at 360 nm (Fig. S2†) revealed that at pH 10, the HBP/LDH = 2/1 solution emitted weaker fluorescence, which gradually intensified after neutralizing and acidifying the pH and even surpassed the fluorescence intensity of the pristine HBP solution. It is noteworthy that the observed changes can be attributed to the release of intercalated HBP upon LDH disintegration in environments with pH levels below 5. The structures of the synthesized LDHs were sensitive to pH variations. When exposed to acidic conditions with a pH below 5, LDH dissolution occurs, leading to the disintegrated of LDH layers into Mg^{2+} and Al^{3+} salts that dissolve in water.[40] Consequently, HBP embedded within the LDH can be released as the LDH disintegrates at pH 4, resulting in an increased fluorescence intensity. This is evidenced by the enhanced fluorescence intensity at pH 4 (red line) compared to pH 7 (blue line) and pH 10 (green line) for HBP/LDH samples with ratios of (a) 2/1, (b) 1/1, and (c) 1/2 in Fig. 4. This observation is also consistent with the findings in Section 3.1.3, where it was noted that the intercalation of HBPs into LDHs substantially weakens HBP fluorescence. This attenuation is attributed to the LDH

interlayers obstructing the fluorescence of the HBP. Furthermore, the reverse process of intercalation and subsequent disintegration of the LDH represents a useful pH-sensitive and self-destructive mechanism for controlling and releasing intercalated HBP molecules. As shown in Fig. 4, at HBP/LDH = 1/1 and 1/2, when the solution was acidified (pH 4), the fluorescence intensity only partially recovered to that of the pristine HBP solution, which can be attributed to the reduced HBP proportion or increased LDH proportion. Although acidification gradually detached the LDH layers, the layers did not completely disappear. Therefore, the fluorescence gradually appears but does not fully manifest, resulting in fluorescence weaker than that of the acidic (pH 4) intercalated solution (HBP/LDH = 2/1).

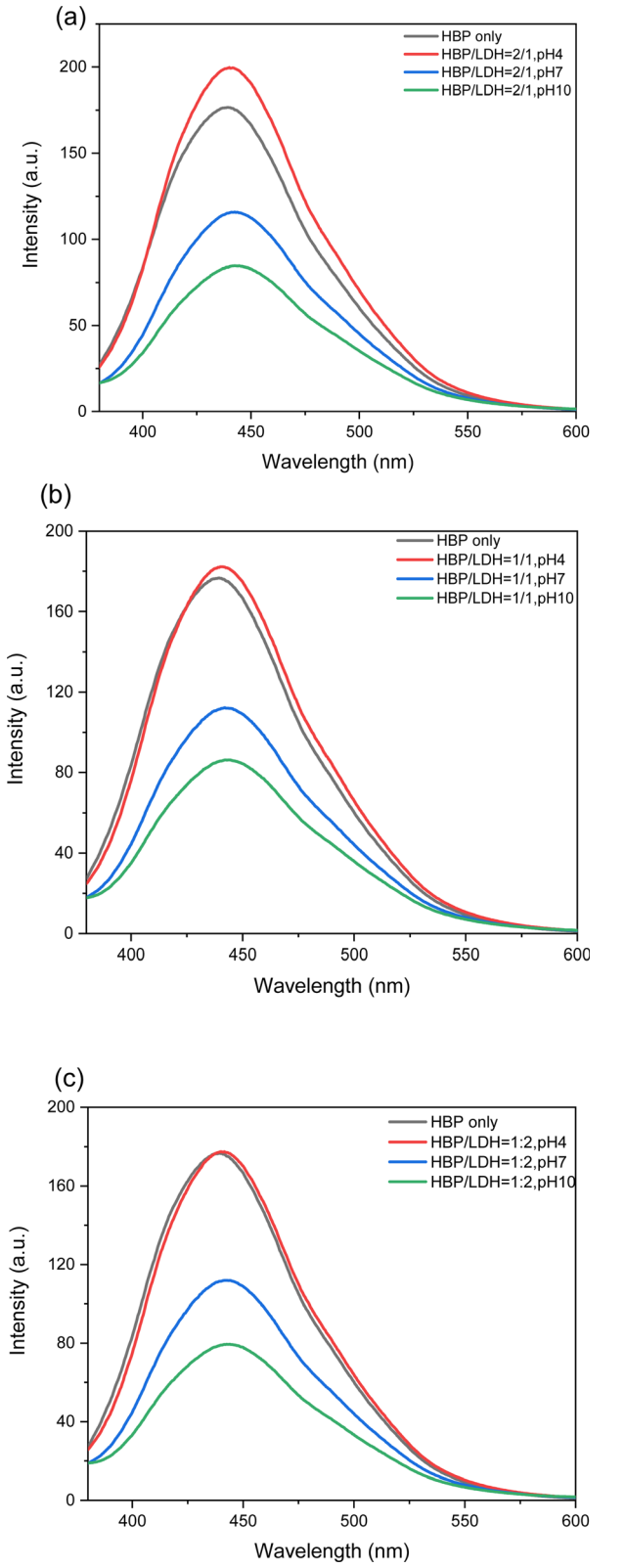

Fig. 4 Photoluminescence of HBP/LDH = (a) 2/1; (b) 1/1; (c) 1/2 solutions.

3.3 QYs of HBP/LDH solutions

The QYs of the aqueous HBP/LDH solutions (pH 10) intercalated at different weight ratios were measured at the optimal excitation of 360 nm. Quinine sulfate, possessing a QY of 54%, was employed as a standard.[41–43] By incorporating photoluminescence and UV-vis spectral data into eqn (1) for calculating QYs, the fluorescence QYs of the HBP/LDH = 2/1, 1/1, and 1/2 solutions (original solution, pH 10) were 0.80, 0.82, and 0.77%, respectively, all within the error range.

Furthermore, by adjusting the pH to gradually strip the LDH layers in neutral and acidic solutions, the QY progressively increased (Table 1). For the neutral (pH 7) HBP/LDH = 2/1, 1/1, and 1/2 solutions, the QYs were 1.04, 1.02, and 1.02%, respectively. Further acidifying the HBP/LDH = 2/1, 1/1, and 1/2 solutions (pH 4) gradually recovered the QYs to 1.73, 1.60, and 1.57%, respectively, approximately double the QY of the original HBP solution (pH 10) and confirming that acidification gradually detaches LDH layers without them completely disappearing. This enabled the QY to gradually recover but not fully return to the QY of the original HBP solution.[30]

3.4 HBP/LDH particle sizes

According to dynamic light scattering measurements,[44] the average particle sizes of the HBP/LDH = 2/1, 1/1, and 1/2 (w/w) solutions were in the range of approximately 100–300 nm (Fig. S4†). In comparison, the average particle size of the pristine LDHs was approximately 300–400 nm. Because of their inherent charge and hydrophilic functional groups, HBPs enhanced the dispersion and reduced the aggregation of LDHs during intercalation. Consequently, the intercalated particles were slightly smaller than the pristine LDHs.

Table 1 QYs of HBP/LDH solutions

Sample	pH	QY (%)
HBP/LDH = 2/1	10	0.80
	7	1.04
	4	1.73
HBP/LDH = 1/1	10	0.82
	7	1.02
	4	1.60
HBP/LDH = 1/2	10	0.77
	7	1.02
	4	1.57

3.5 Images of HBP/LDH

As shown in Fig. 5(a–c), the TEM images of HBP/LDH = 2/1, 1/1, and 1/2 (w/w), respectively, show a singular lamellar structure, suggesting that when different weight ratios of HBPs intercalated LDHs, the HBPs embedded in the LDH interlayer and promoted anion exchange. Consequently, the HBPs were encapsulated in the LDHs, transforming the larger aggregated LDH lamellar structure to smaller, individual lamellar structures.

3.6 Antibacterial activity assay

3.6.1 Antibacterial activity of HBPs. We used different pH values and HBP concentrations to test the HBP inhibitory activity against *E. coli* pUC19/DH5α. The results indicated that at a concentration of 2^N, as N decreases in a semidilution series, the inhibition zone shrinks, revealing decreased antibacterial activity (Fig. S5(a)†). This is attributed to the highly branched structure, terminal functional groups, and charge of the zwitterionic HBPs,[11,45] enabling HBPs to inhibit bacterial growth. However, at 4 mg mL^{-1} of HBPs and different pH values, the pH negligibly altered the size of the inhibition zone at the same HBP concentration (Fig. S5(b)†). Hence, the antibacterial effectiveness of HBPs remained relatively constant at the same concentration, irrespective of the pH. One of the proposed antibacterial mechanisms is driven by the membrane-disruptive properties of these cationic surfactants, which interact with the negatively charged bacterial cell wall through their abundant cationic groups. This interaction compromises the integrity of the cell wall, leading to its rupture and ultimately resulting in cell death. The membrane-disruptive characteristics of these cationic surfactants have been confirmed through enzymatic assays involving *E. coli* and are considered a primary mechanism underlying their antibacterial activity.[46–48] This is consistency with our HBPs possess the peripheral functional groups of amino ($-NH_3^+$) cationic groups with observed antibacterial properties.

3.6.2 Antibacterial activity of HBP-intercalated LDHs. Subsequently, we investigated the antibacterial activities of HBP/LDH intercalated at various weight ratios (w/w). We have performed the inhibition zone measurements from the first test (I) for each day observation and second formal runs (II). The raw data of first test run reflects inhibition zones of both the raw HBP and HBP/LDH samples, observed from day 1 through day 5 across three replicate experiments with varying HBP/LDH weight ratios. In the first run (I), the experiment concluded on day 5 as the pristine HBP solution became fully overgrown with bacteria, leading the inhibition zones indistinguishable. In contrast, the HBP/LDH intercalated solutions exhibited gradual expansion of the inhibition zones, which led us to perform the second formal experiment. Fig. 6 represents the results from the second run (II), where data was collected on days 1, 3, and 5, informed by the observations made in the first run. On the first day, the intercalated solutions exhibited smaller inhibition zones compared to the pristine HBP solution at the same concentration (Fig. 6(a) and (b)). However, by the fifth day, the inhibition zones of the intercalated solutions gradually expanded. In contrast, on the fifth day, the inhibition zone of the pristine HBP solution was fully overgrown with bacteria, indicating that the HBP/LDH antibacterial activity was slowly released over time and that compared with the pristine HBP solution, the HBP/LDH solutions maintained their antibacterial effects for an extended period, demonstrating a sustained-release application (Fig. 6(c)–(f)). To further quantify the antibacterial activity of HBP, we employed ImageJ software to analyze the inhibition zone area (in arbitrary units, AU). This analysis enabled us to establish a correlation between HBP concentration and the inhibition zone area. A linear relationship was identified between HBP concentrations of 4, 8, 16, and 32 mg mL^{-1} and their corresponding inhibition zone areas, as represented by the equation $Y = 21.0X + 170.0$ (Fig. 7). This finding demonstrates that higher HBP concentrations result in larger clear inhibition zones, offering a quantitative approach for evaluating the antibacterial activity of HBP through ImageJ analysis.

3.7 Cell viability assay

We used MTT assays to evaluate the cellular viability of the HBP/LDH = 2/1. According to the medical device biocompatibility standard (ISO 10993) *in vitro* cytotoxicity test, if the cell viability is below 70%, the device is potentially cytotoxic. In this study, a standard for maintaining cell viability above 80% was set to assess whether HBP/LDH exhibited reduced cytotoxicity. Various concentrations (0, 50, 100, 300, and 500 μg mL^{-1}) of HBP/LDH were tested for toxicity against human keratinocytes

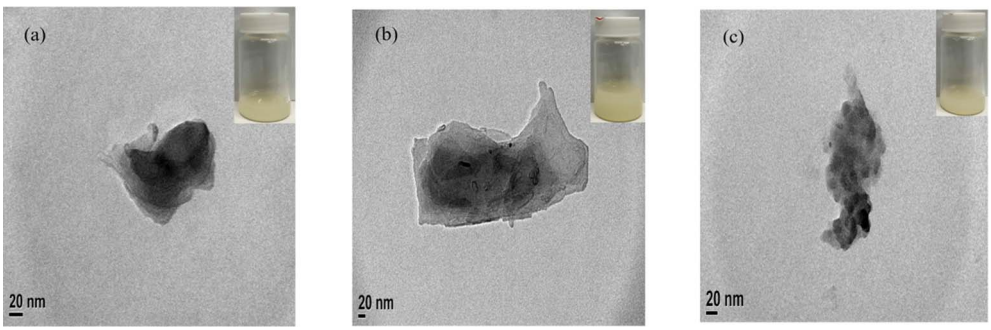

Fig. 5 TEM images of HBP/LDH = (a) 2/1; (b) 1/1; (c) 1/2.

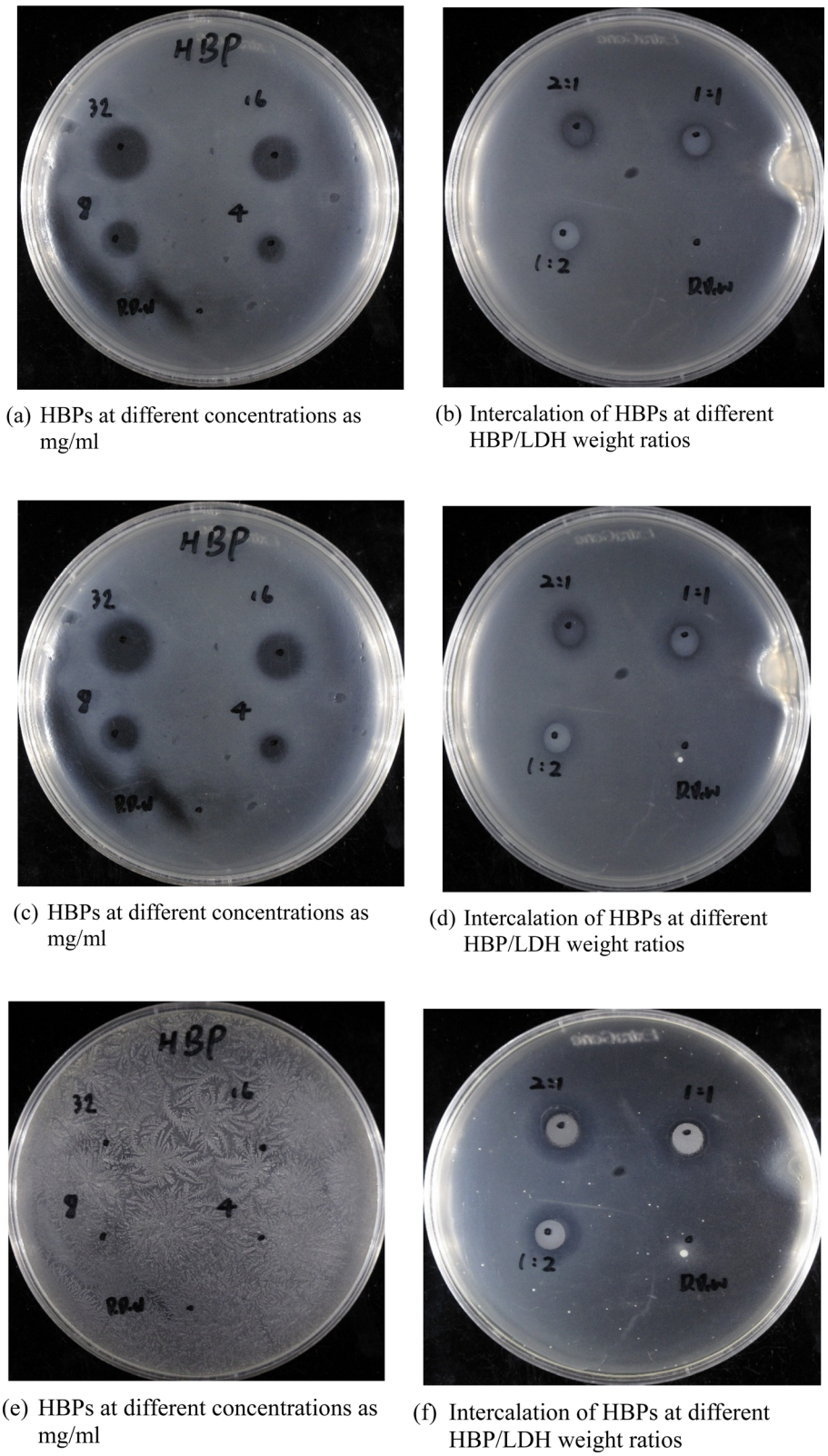

(a) HBPs at different concentrations as mg/ml

(b) Intercalation of HBPs at different HBP/LDH weight ratios

(c) HBPs at different concentrations as mg/ml

(d) Intercalation of HBPs at different HBP/LDH weight ratios

(e) HBPs at different concentrations as mg/ml

(f) Intercalation of HBPs at different HBP/LDH weight ratios

Fig. 6 Inhibition zones of (a, c and e) pristine HBPs and (b, d and f) HBP/LDH at different HBP/LDH weight ratios at days (a and b) 1; (c and d) 3; (e and f) 5.

HaCaT cells for 24 h. The results demonstrated that at all the concentrations, HBP/LDH exhibited extremely high cell viabilities. Even at the highest HBP/LDH concentration of 500 μg mL^{-1}, the cell viability remained above 80%, indicating low cytotoxicity. Skin HaCaT cells were treated with HBP/LDH for 24 h to assess whether HBP/LDH could induce short-term

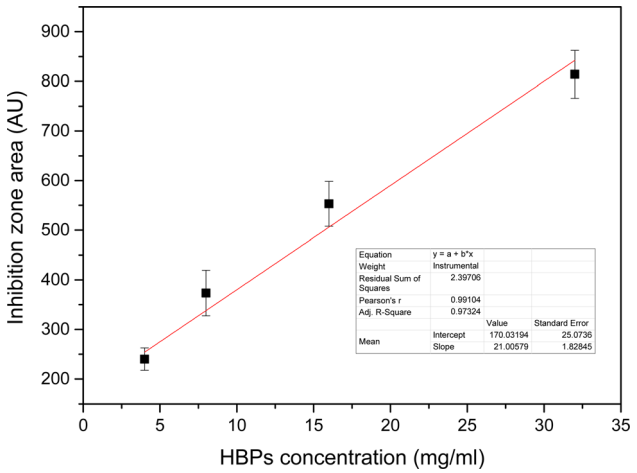

Fig. 7 The relationship between HBP concentration and their corresponding inhibition zone area as function of $Y = 21.0X + 170.0$.

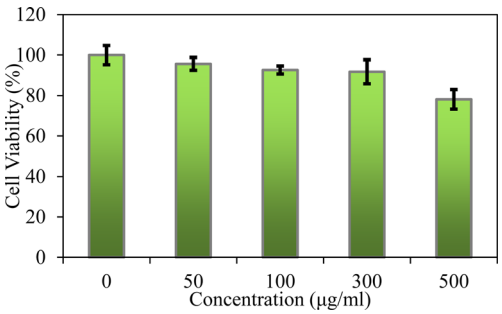

Fig. 8 Effects of HBP/LDH = 2/1 on skin HaCaT cell viability.

toxicity. These results indicate the potential combination of HBP/LDH with drugs for application to wound dressings or drug delivery carriers (Fig. 8).

4 Conclusions

This study investigated the preparation and analysis of HBPs and LDHs and examined their structures and properties. Additionally, LDHs were used as a layered carrier, various weight ratios of HBPs intercalated between the LDH layers through intermolecular forces, and the subsequent structural transformations were observed. The HBP/LDH characteristics were identified, and the antibacterial activity was investigated as follows: the structures and characteristics of the HBPs and LDHs were determined through various analyses. The HBPs exhibited an average particle size ranging from 10 to 30 nm, and TEM images revealed that the HBPs possessed a spherical morphology. XRD patterns indicated that the LDH interlayer spacing was extended from 8.0 to approximately 24 Å or more for HBP/LDH. FTIR spectra revealed that HBPs comprised carboxyl and amino functional groups, while LDHs exhibited signals corresponding to O–H and NO_3^- stretching peaks. Furthermore, the HBP antimicrobial tests revealed the generation of an inhibition zone, which size increased with increasing HBP concentration, indicating that HBPs possessed antimicrobial activity.

Next, different weight ratios (w/w) of HBPs were intercalated into the LDH interlayer, and the HBP/LDHs were characterized. XRD patterns revealed an expanded interlayer spacing ranging from 21.8 to 25.5 Å compared to the original LDH interlayer spacing of 8.6 Å. This allows for the intercalation of HBPs into the LDH interlayer and subsequent expansion of the interlayer spacing. After intercalation, TEM images showed a change in the original sheet-like structure of the LDHs, indicating deformation caused by the intercalation of the HBPs into the interlayer. Lastly, the HBP/LDH intercalated nanohybrids employed in antimicrobial activity tests possessed antimicrobial capabilities. Subsequent cytotoxicity assays revealed that HBP/LDH exhibited low cytotoxicity on human keratinocytes HaCaT cell. Compared with HBPs, the intercalated material evidently exhibited a prolonged and controllable release of antimicrobial agents over 5 days, implying the potential combination of HBP/LDH with drugs for application to antimicrobial wound dressings or biocompatible drug delivery carriers.

Data availability

The data supporting this article have been included as part of the ESI.†

Author contributions

All authors had full access to all the data in the study and take responsibility for the integrity of the data and the accuracy of the data analysis. Data curation and methodology, C.-K. Liu, F.-Y. Su, conceptualization, writing—original draft preparation; writing—review and editing, project administration, T.-Y. Juang, Y.-C. Liu.

Conflicts of interest

None of the authors have conflicts of interests relevant to this article.

Acknowledgements

Funding/Support: NSTC 112-2221-E-039-006-MY2, CMU111-S-08, CMU111-ASIA-11, CMU112-MF-66.

References

1 W. He, Y. Gan, X. Qi, H. Wang, H. Song, P. Su, J. Song and Y. Yang, Enhancing Enzyme Activity Using Hydrophilic Hollow Layered Double Hydroxides as Encapsulation Carriers, *ACS Appl. Mater. Interfaces*, 2023, **15**(29), 34513–34526.

2 C. Zhou, J. Chen, B. Zheng, P. Zhu, Q. Chu, F. Li, Y. Fu, X. Li and J. Luo, Integration of CoAl-Layered Double Hydroxides on Commensal Bacteria to Enable Targeted Tumor Inhibition and Immunotherapy, *ACS Appl. Mater. Interfaces*, 2023, **15**(38), 44731–44741.

3 H. Qi, K. Huang, F. Pan, R. Ma, C. Lian, H. Liu and J. Hu, Boosting Direct Seawater Electrolysis through Intercalation Engineering of Layered Double Hydroxides, *Ind. Eng. Chem. Res.*, 2023, **62**(46), 19674–19682.
4 T. Hu, Z. Gu, G. R. Williams, M. Strimaite, J. Zha, Z. Zhou, X. Zhang, C. Tan and R. J. C. S. R. Liang, Layered double hydroxide-based nanomaterials for biomedical applications, *Chem. Soc. Rev.*, 2022, **51**(14), 6126–6176.
5 H. Asiabi, Y. Yamini, M. Alipour, M. Shamsayei and S. Hosseinkhani, Synthesis and characterization of a novel biocompatible pseudo-hexagonal NaCa-layered double metal hydroxides for smart pH-responsive drug release of dacarbazine and enhanced anticancer activity in malignant melanoma, *Mater. Sci. Eng., C*, 2019, **97**, 96–102.
6 C. Taviot-Guého, V. Prévot, C. Forano, G. Renaudin, C. Mousty and F. Leroux, Tailoring hybrid layered double hydroxides for the development of innovative applications, *Adv. Funct. Mater.*, 2018, **28**(27), 1703868.
7 M. Chen, R. Bi, R. Zhang, F. Yang and F. Chen, Tunable surface charge and hydrophilicity of sodium polyacrylate intercalated layered double hydroxide for efficient removal of dyes and heavy metal ions, *Colloids Surf., A*, 2021, **617**, 126384.
8 A. Kavand, N. Anton, T. Vandamme, C. A. Serra and D. Chan-Seng, Synthesis and functionalization of hyperbranched polymers for targeted drug delivery, *J. Controlled Release*, 2020, **321**, 285–311.
9 A. K. Gayen, R. Singla and S. Ramakrishnan, Hyperbranched polymers: growing richer in flavours with time, *Chem. Commun.*, 2024, **60**(12), 1534–1545.
10 S. Shen, Y. wu, Y. Liu and D. wu, High drug-loading nanomedicines: progress, current status, and prospects, *Int. J. Nanomed.*, 2017, **12**, 4085–4109.
11 M. Li, B. Zhuang and J. Yu, Functional Zwitterionic Polymers on Surface: Structures and Applications, *Chem.–Asian J.*, 2020, **15**(14), 2060–2075.
12 M. Li, B. Zhuang and J. Yu, Sequence–Conformation Relationship of Zwitterionic Peptide Brushes: Theories and Simulations, *Macromolecules*, 2021, **54**(20), 9565–9576.
13 K. Ulbrich, K. Holá, V. Šubr, A. Bakandritsos, J. Tuček and R. Zbořil, Targeted drug delivery with polymers and magnetic nanoparticles:Covalent and noncovalent approaches, release control, and clinicalstudies, *Chem. Rev.*, 2016, **116**(9), 5338–5431.
14 J. Yan, X. Wang, J. Xiong, L. Wang, D. Pan, Y. Xu and M. Yang, Uncovering divergent fluorescence of aliphatic polyamides: Synthesis, dual polymerization-induced emissions, and organelle-specific imaging, *Chem. Eng. J.*, 2022, **428**, 132142.
15 X. Bi, H. Zhang and L. Dou, Layered double hydroxide-based nanocarriers for drug delivery, *Pharmaceutics*, 2014, **6**(2), 298–332.
16 K.-H. Goh, T.-T. Lim and Z. Dong, Application of layered double hydroxides for removal of oxyanions: a review, *Water Res.*, 2008, **42**(6–7), 1343–1368.
17 G. Mishra, B. Dash and S. Pandey, Layered double hydroxides: A brief review from fundamentals to application as evolving biomaterials, *Appl. Clay Sci.*, 2018, **153**, 172–186.
18 S.-C. Kan, C.-C. Lee, Y.-C. Hsu, Y.-H. Peng, C.-C. Chen, J.-J. Huang, J.-W. Huang, C.-J. Shieh, T.-Y. Juang and Y.-C. Liu, Enhanced surfactin production *via* the addition of layered double hydroxides, *J. Taiwan Inst. Chem. Eng.*, 2017, **80**, 10–15.
19 Y.-C. Hsu, P.-H. Chang, C.-N. Lin, C.-Y. Li, T.-Y. Juang and Y.-C. Liu, A fermentation process for the *in situ* intercalation of surfactin into layered double hydroxides, *Appl. Clay Sci.*, 2019, **182**, 105247.
20 N. Morel-Desrosiers, J. Pisson, Y. Israëli, C. Taviot-Guého, J.-P. Besse and J.-P. Morel, Intercalation of dicarboxylate anions into a Zn–Al–Cl layered double hydroxide: microcalorimetric determination of the enthalpies of anion exchange, *J. Mater. Chem.*, 2003, **13**(10), 2582–2585.
21 M. T. Rahman, T. Kameda, S. Kumagai and T. Yoshioka, A novel method to delaminate nitrate-intercalated MgAl layered double hydroxides in water and application in heavy metals removal from waste water, *Chemosphere*, 2018, **203**, 281–290.
22 M. Sajid, C. Basheer, K. Narasimhan, A. Buhmeida, M. Al Qahtani and M. S. J. N. E. Al-Ahwal, Persistent and endocrine disrupting organic pollutants: advancements and challenges in analysis, health concerns and clinical correlates, *Nat., Environ. Pollut. Technol.*, 2016, **15**(2), 733.
23 B. Vishnu, S. Sriram and J. Jayabharathi, A green synthetic approach: crystalline–amorphous interface CoFe-LDH as a sustainable electrocatalyst for water oxidation with low cell voltage and evaluation of its sustainability standards, *Sustainable Energy Fuels*, 2023, **7**(18), 4638–4653.
24 H. Asiabi, Y. Yamini, M. Alipour, M. Shamsayei and S. Hosseinkhani, Synthesis and characterization of a novel biocompatible pseudo-hexagonal NaCa-layered double metal hydroxides for smart pH-responsive drug release of dacarbazine and enhanced anticancer activity in malignant melanoma, *Mater. Sci. Eng., C*, 2019, **97**, 96–102.
25 S. B. Khan, K. A. Alamry, N. A. Alyahyawi and A. M. Asiri, Controlled release of organic–inorganic nanohybrid: cefadroxil intercalated Zn–Al-layered double hydroxide, *Int. J. Nanomed.*, 2018, **13**, 3203.
26 W. Dong, Y. Zhou, D. Yan, H. Li and Y. Liu, pH-responsive self-assembly of carboxyl-terminated hyperbranched polymers, *Phys. Chem. Chem. Phys.*, 2007, **9**(10), 1255–1262.
27 F. Xu, J. Zhong, X. Qian, Y. Li, X. Lin and Q. Wu, Multifunctional poly (amine-ester)-type hyperbranched polymers: lipase-catalyzed green synthesis, characterization, biocompatibility, drug loading and anticancer activity, *Polym. Chem.*, 2013, **4**(12), 3480–3490.
28 F. Prinetto, G. Ghiotti, P. Graffin and D. Tichit, Synthesis and characterization of sol–gel Mg/Al and Ni/Al layered double hydroxides and comparison with co-precipitated samples, *Microporous Mesoporous Mater.*, 2000, **39**(1–2), 229–247.
29 H. Chen and J. Kong, Hyperbranched polymers from A 2+ B 3 strategy: Recent advances in description and control of fine topology, *Polym. Chem.*, 2016, **7**(22), 3643–3663.

30 Y.-Y. Chen, S.-C. Fan, C.-C. Chang, J.-C. Wang, H.-M. Chiang and T.-Y. Juang, Non-Conventional Fluorescence and Cytotoxicity of Two Aliphatic Hyperbranched Polymer Dots Having Poly (amic acid) Structures: Implications for Labeling Nanodrug Carriers, *ACS Omega*, 2021, **6**(48), 33159–33170.

31 J. Liao, Z. Cheng and L. Zhou, Nitrogen-doping enhanced fluorescent carbon dots: green synthesis and their applications for bioimaging and label-free detection of Au3+ ions, *ACS Sustain. Chem. Eng.*, 2016, **4**(6), 3053–3061.

32 H. Khan, A. S. Yerramilli, A. D'Oliveira, T. L. Alford, D. C. Boffito and G. S. Patience, Experimental methods in chemical engineering: X-ray diffraction spectroscopy—XRD, *Can. J. Chem. Eng.*, 2020, **98**(6), 1255–1266.

33 M. Zaidan, A. Noor Rain, A. Badrul, A. Adlin, A. Norazah and I. Zakiah, In vitro screening of five local medicinal plants for antibacterial activity using disc diffusion method, *Trop. Biomed.*, 2005, **22**(2), 165–170.

34 X. Yuan, Z. Liu, Z. Guo, Y. Ji, M. Jin and X. Wang, Cellular distribution and cytotoxicity of graphene quantum dots with different functional groups, *Nanoscale Res. Lett.*, 2014, **9**(1), 1–9.

35 P. Ramachandran, C. Y. Lee, R.-A. Doong, C. E. Oon, N. T. K. Thanh and H. L. Lee, A titanium dioxide/nitrogen-doped graphene quantum dot nanocomposite to mitigate cytotoxicity: synthesis, characterisation, and cell viability evaluation, *RSC Adv.*, 2020, **10**(37), 21795–21805.

36 Y. N. Chan, T. Y. Juang, Y. L. Liao, S. A. Dai and J. J. Lin, Preparation of clay/epoxy nanocomposites by layered-double-hydroxide initiated self-polymerization, *Polymer*, 2008, **49**(22), 4796–4801.

37 S.-M. Shau, T.-Y. Juang, H.-S. Lin, C.-L. Huang, C.-F. Hsieh, J.-Y. Wu and R.-J. Jeng, Individual graphene oxide platelets through direct molecular exfoliation with globular amphiphilic hyperbranched polymers, *Polym. Chem.*, 2012, **3**(5), 1249–1259.

38 S.-M. Shau, T.-Y. Juang, H.-S. Lin, C.-L. Huang, C.-F. Hsieh, J.-Y. Wu and R.-J. Jeng, Individual graphene oxide platelets through direct molecular exfoliation with globular amphiphilic hyperbranched polymers, *Polym. Chem.*, 2012, **3**, 1249–1259.

39 M. Shabanian, M. Hajibeygi, and A. Raeisi, FTIR characterization of layered double hydroxides and modified layered double hydroxides, in *Layered Double Hydroxide Polymer Nanocomposites*, Elsevier, 2020, pp. 77–101.

40 C.-W. Chiu, Y.-L. Liao and J.-J. Lin, Mg–Al Layered Double Hydroxides Intercalated with Polyetheramidoacids and Exhibiting a pH-Responsive Releasing Property, *Ind. Eng. Chem. Res.*, 2012, **51**(1), 581–586.

41 H. Zhu, X. Wang, Y. Li, Z. Wang, F. Yang and X. Yang, Microwave synthesis of fluorescent carbon nanoparticles with electrochemiluminescence properties, *Chem. Commun.*, 2009, (34), 5118–5120.

42 B. De and N. Karak, A green and facile approach for the synthesis of water soluble fluorescent carbon dots from banana juice, *RSC Adv.*, 2013, **3**(22), 8286–8290.

43 I. Grabchev, P. Bosch, M. McKenna and D. Staneva, A new colorimetric and fluorimetric sensor for metal cations based on poly (propilene amine) dendrimer modified with 1, 8-naphthalimide, *J. Photochem. Photobiol., A*, 2009, **201**(1), 75–80.

44 T. Qiang, Q. Bu, Z. Huang and X. Wang, Synthesis and characterization of hyperbranched linear surfactants, *J. Surfactants Deterg.*, 2014, **17**, 215–221.

45 Q. Liu, W. Li, H. Wang, B.-m. Z. Newby, F. Cheng and L. Liu, Amino Acid-Based Zwitterionic Polymer Surfaces Highly Resist Long-Term Bacterial Adhesion, *Langmuir*, 2016, **32**(31), 7866–7874.

46 S. Roy, I. Hasan and B. Guo, Recent advances in nanoparticle-mediated antibacterial applications, *Coord. Chem. Rev.*, 2023, **482**, 215075.

47 N. Bag, S. Bardhan, S. Roy, J. Roy, D. Mondal, B. Guo and S. Das, Nanoparticle-mediated stimulus-responsive antibacterial therapy, *Biomater. Sci.*, 2023, **11**(6), 1994–2019.

48 H. Huang, A. Ali, Y. Liu, H. Xie, S. Ullah, S. Roy, Z. Song, B. Guo and J. Xu, Advances in image-guided drug delivery for antibacterial therapy, *Adv. Drug Delivery Rev.*, 2023, **192**, 114634.